

# Room temperature spin-polarizations of Mn-based antiferromagnetic nanoelectrodes

Cite as: Appl. Phys. Lett. **105**, 183109 (2014); <https://doi.org/10.1063/1.4901047>

Submitted: 31 August 2014 . Accepted: 21 October 2014 . Published Online: 06 November 2014

Toyo Kazu Yamada, and Amadeo L. Vazquez de Parga



View Online



Export Citation



CrossMark

## ARTICLES YOU MAY BE INTERESTED IN

[Electron-bombarded  \$\langle 110 \rangle\$ -oriented tungsten tips for stable tunneling electron emission](#)  
Review of Scientific Instruments **87**, 033703 (2016); <https://doi.org/10.1063/1.4943074>

[Use of voltage pulses to detect spin-polarized tunneling](#)  
Applied Physics Letters **82**, 1437 (2003); <https://doi.org/10.1063/1.1556958>

[Bulk Cr tips with full spatial magnetic sensitivity for spin-polarized scanning tunneling microscopy](#)  
Applied Physics Letters **97**, 083104 (2010); <https://doi.org/10.1063/1.3474659>

**HIDEN**  
ANALYTICAL

Instruments for **Advanced Science**

- Knowledge,
- Experience,
- Expertise

[Click to view our product catalogue](#)

Contact Hiden Analytical for further details:

[www.HidenAnalytical.com](http://www.HidenAnalytical.com)  
[info@hiden.co.uk](mailto:info@hiden.co.uk)



**Gas Analysis**

- ▶ dynamic measurement of reaction gas streams
- ▶ catalysis and thermal analysis
- ▶ molecular beam studies
- ▶ dissolved species probes
- ▶ fermentation, environmental and ecological studies



**Surface Science**

- ▶ UHVTPD
- ▶ SIMS
- ▶ end point detection in ion beam etch
- ▶ elemental imaging - surface mapping



**Plasma Diagnostics**

- ▶ plasma source characterization
- ▶ etch and deposition process reaction kinetic studies
- ▶ analysis of neutral and radical species



**Vacuum Analysis**

- ▶ partial pressure measurement and control of process gases
- ▶ reactive sputter process control
- ▶ vacuum diagnostics
- ▶ vacuum coating process monitoring

**AIP**  
Publishing

## Room temperature spin-polarizations of Mn-based antiferromagnetic nanoelectrodes

Toyo Kazu Yamada<sup>1,a)</sup> and Amadeo L. Vazquez de Parga<sup>2</sup>

<sup>1</sup>Graduate School of Advanced Integration Science, Chiba University, 1-33, Yayoi-cho, Inage-ku, Chiba-shi 263-8522, Chiba, Japan

<sup>2</sup>Instituto Madrileño de Estudios Avanzados en Nanociencia IMDEA-Nanociencia and Dep. Física de la Materia Condensada, Universidad Autónoma de Madrid, Cantoblanco, 28049 Madrid, Spain

(Received 31 August 2014; accepted 21 October 2014; published online 6 November 2014)

Antiferromagnets produce no stray field, and therefore, a tip electrode made of antiferromagnetic material has been considered to be the most suitable choice to measure such as magnetoresistance (MR) through single isolated magnetic nanoparticles, molecules, and ultrathin films. Spin polarizations ( $P$ ) of antiferromagnetic 3-nm, 6-nm, and annealed 3-nm Mn films grown on W tips with a bcc(110) apex as well as bulk-NiMn tips were obtained at 300 K by measuring MR in ultra-high vacuum by means of spin-polarized scanning tunneling microscopy using a layerwise antiferromagnetically stacked bct-Mn(001) film electrode. The Mn-coated tips with coverages of 3 and 6 nm exhibited  $P$  values of  $1 \pm 1\%$  and  $3 \pm 2\%$ , respectively, which tips likely contain  $\alpha$ - or strained Mn. With a thermal assist, the crystalline quality and the magnetic stability of the film could increase. The annealed tip exhibited  $P = 9 \pm 2\%$ . The bulk-NiMn tips exhibit spin polarizations of 0 or  $6 \pm 2\%$  probably depending on the chemical species (Mn or Ni) present at the apex of the tip. Fe-coated W tips were used to estimate the bct-Mn(001) film spin polarization. © 2014 Author(s). All article content, except where otherwise noted, is licensed under a Creative Commons Attribution 3.0 Unported License. [<http://dx.doi.org/10.1063/1.4901047>]

The miniaturization of electronic devices has been considered to be a key solution to realize novel nanodevices with low energy consumption, low cost, and high performance to cater to the increasing demands of data storage and retrieval. Unique electron-spin properties have been observed in exotic materials at atomically small-scale, yielding applications such as electric-field control spintronics with ultrathin magnetic films,<sup>1-3</sup> 1-nm-size single organic molecular magnetoresistance sensors,<sup>4-6</sup> and graphene-based spintronics.<sup>7</sup>

Scanning tunneling microscopy (STM) is considered as a powerful tool to precisely measure spin information, e.g., spin-polarization or magnetoresistance (MR), of 1-nm-size nanomagnets or atomically thin magnetic films.<sup>3-5,8</sup> Figure 1(a) shows a sketch of STM magnetic junctions, in which electrode (1) is the magnetic tip and electrode (2) is the magnetic sample. Ferromagnetic (FM) Fe-coated W tips have been used only for studying nanomagnets with higher anisotropies (e.g., Fe thin-films on W(110)<sup>9</sup> and Co bilayer islands on Cu(111)<sup>4,10</sup>) or antiferromagnetic (AFM) samples (e.g., Mn(001) ultrathin films<sup>11-14</sup> and Cr(001) surfaces<sup>15</sup>). However, if the magnetic nanostructure under study has a small magnetic anisotropy, the spin structure may be easily affected by external magnetic fields,<sup>16</sup> and therefore, the use of FM tips should be avoided because they produce a considerable stray field.<sup>17,18</sup> As opposed to ferromagnets, antiferromagnets exhibit no stray field, and therefore, a tip made of AFM material has been considered to be the best choice to image single isolated magnetic nanoparticles or single magnetic molecules. Tips made of AFM material have already

been fabricated and used in STM experiments in recent years, e.g., bulk-Cr,<sup>19,20</sup> Cr-coated,<sup>18,21,22</sup> and Mn-coated W tips.<sup>23</sup> The fabrication techniques of Cr-based AFM tips have been

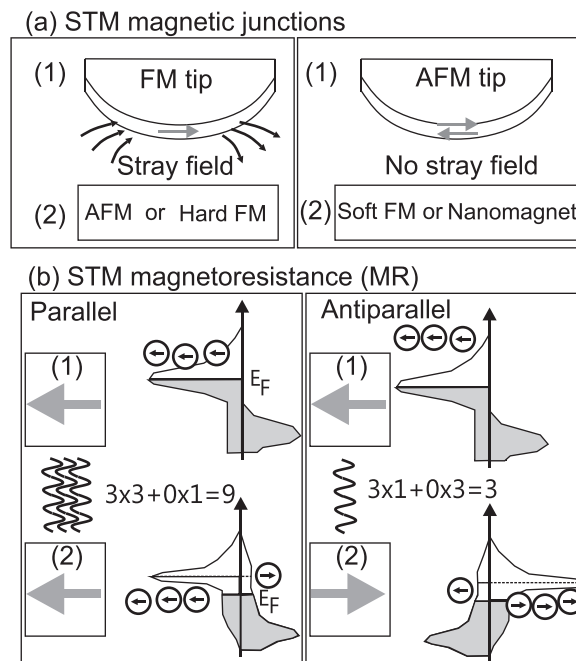


FIG. 1. (a) STM magnetic junctions. The STM tip probe detects spin-polarization as well as the magnetoresistance (spin-polarized conductance) through the junction. A ferromagnetic (FM) tip has a stray field, but an antiferromagnetic (AFM) tip has no stray field. (b) A simple model of electron spin tunneling between two magnets through a spacer gap. Grey arrows denote magnetization vectors. Black arrows indicate up and down spins. Here, we assume that 3 up-spins exist for the electrode (1) and 3 up- and 1 down-spins exist for the electrode (2) at the Fermi energy.

<sup>a)</sup>Email: toyoyamada@faculty.chiba-u.jp. Tel.: 81-432903915.

investigated in detail. In one such study, the spin polarization of the apex of the Cr/W tip was measured to be  $\sim 10\%$  at 300 K.<sup>22</sup> However, the MR as well as spin polarization of Mn-based AFM tip electrodes has not been examined in detail.

In this study, quantitative 300-K spin polarization values of Mn-based AFM tip electrodes were obtained by measuring MR values with a spin-polarized STM setup in ultra-high vacuum (UHV). Mn-coated W and bulk-NiMn tips were used in our experiments. Fe-coated W tips<sup>11,12,25</sup> were used to estimate the sample spin polarization.

Thin bct-Mn(001) films epitaxially grown on Fe(001) whiskers with Curie temperatures higher than 300 K were used as magnetic samples.<sup>24</sup> A clean and atomically flat bcc-Fe(001) surface was obtained on single crystal Fe whiskers via several cycles of Ar<sup>+</sup> sputtering and annealing up to 870 K. Mn(001) ultrathin films were grown on clean Fe(001) surfaces whose temperatures were maintained at 370 K during the Mn deposition.

Mn films grown on the Fe(001) thicker than four layers have an equivalent bct structure with in-plane and out-of-plane atomic lattice distances of 0.287 and 0.165 nm, respectively ( $c/a = 1.15$ ).<sup>24</sup> Although intermixing was observed up to the third layer, the films thicker than four layers consist of only pure Mn atoms. Also, each Mn layers above the fourth layer have the same local density of states.<sup>24</sup> Concentration of impurities on the Mn(001) surface was less than 1%. Since the contrast in the STM spectroscopy maps may have its origin in different local density of states, different chemical species, and different spin polarizations, the bct-Mn(001) films thicker than four layers are considered to be one of the test samples to check spin contrast.<sup>11–14</sup> In this study, we used fifth (“5”) and sixth (“6”) layers of the Mn films to check the spin contrast.

The W tips were electrochemically etched from W wires (diameter 0.3 mm, purity 99.9%) in air using aqueous KOH, and subsequently, the tip was rinsed with hot water and transferred into the load lock chamber of our STM setup. Once in UHV, the apex of the W tip was sputtered with Ne<sup>+</sup> in UHV and annealed at temperatures up to 2000 K to obtain a clean W apex. Fe-coated W tips were prepared by depositing 5-nm Fe on a clean W tip with a radius of 10–30 nm at 300 K in UHV following the method described in Ref. 25. Mn-coated W tips were prepared by depositing Mn on a clean and blunt W tip in UHV at 300 K. The post-annealing process of the Mn-coated W tip involved contacting a heater filament (10 W) for 5 min at a point at 3 mm below the tip apex. NiMn tips were electrochemically etched (4 V, 20 mA) from NiMn polycrystalline rods (diameter 0.5 mm) using 0.5M HCl aq.

STM and scanning tunneling spectroscopy (STS) experiments were performed at 300 K in UHV with a base pressure of  $< 8 \times 10^{-9}$  Pa. The STS measurements were performed by disconnecting the feedback loop, i.e., fixing the tip-sample separation ( $z$ ) and measuring the tunneling current at each pixel of the corresponding topographic image by varying the sample voltage around the Fermi level.<sup>26</sup> The differential conductivity ( $dI/dV$ ) curves were obtained by numerical differentiation of the corresponding  $I(V)$  curves. Magnetoresistance (MR) measurements were obtained as discussed below. Figure 1(b) shows an example of the electron spin transport through a gap

between two magnets. Grey arrows indicate magnetizations. Black arrows indicate up and down spins. Here, we assume that 3 up-spins exist for the electrode (1) and 3 up- and 1 down-spins exist for the electrode (2) at the Fermi energy, i.e., electrode (1) exhibits only a minority spin peak at the Fermi energy, thereby indicating 100% spin polarization. In the case of parallel coupling, the electron spin transfer probability through the gap is  $3 \times 3 + 1 \times 0 = 9$ . On the other hand, when the coupling is antiparallel, the minority and majority spin states of electrode (2) exhibit a reversal, and the transfer probability is consequently  $3 \times 1 + 0 \times 3 = 3$ , i.e., the conductance ( $G$ ) depends on the type of magnetic coupling. In the case of Fig. 1(b), we obtained an MR of  $(G_{\uparrow\downarrow}^{-1} - G_{\uparrow\uparrow}^{-1})/G_{\uparrow\uparrow}^{-1} = 67\%$ ,<sup>27</sup> wherein the spin polarizations of electrodes (1) and (2) were 100% and 50%, respectively.

First, we obtained the spin-resolved  $dI/dV$  maps with the W tip covered by a 5-nm Fe film. Figure 2(a) shows a cross-sectional model of the Mn(001) films, which were grown on an Fe(001) whisker substrate at 370 K. Due to the growth mode, several Mn layers are exposed at the surface, as can be seen in the STM topographic image shown in Fig. 2(b). Figure 2(c) shows the spectroscopic  $dI/dV$  map measured simultaneously with the topographic image shown in panel (b) with an Fe-covered W tip. The black and white contrast between adjacent Mn terraces is due to the AFM layered structure, and the contrast reflects the spin-dependent electron tunneling probability between the magnetic tip and sample, as shown in Fig. 1(b), i.e., the contrast in the  $dI/dV$  map indicates that the tip electrode has a Curie temperature that is higher than 300 K and also that the MR as well as spin polarization are not zero at 300 K.<sup>26,28</sup> From this contrast, we determine that the 5-nm Fe film on the W tip can be used to measure MR at 300 K.

Figures 3(a)–3(d) show topographic images and the corresponding spin-resolved  $dI/dV$  maps obtained with

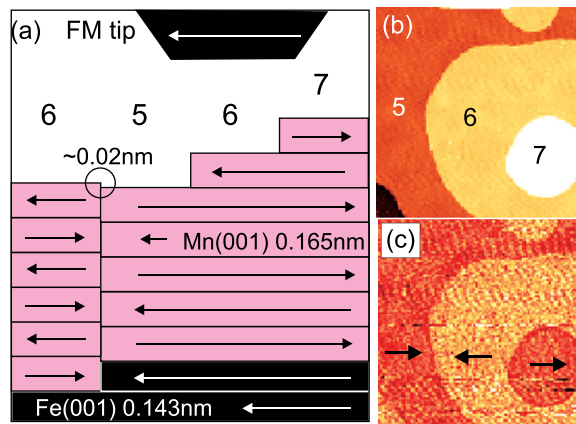


FIG. 2. (a) Model of a spin-polarized STM setup at the surface of layerwise antiferromagnetic stacking bct-Mn(001) layers grown on Fe(001) whisker with a FM tip. Arrows indicate directions of spin polarization vectors. Numbers denote the stacking number of the Mn monolayers at each position. Interlayer spacing of the Mn films thicker than fourth layer is 0.165 nm.<sup>24</sup> A hidden Fe step was also observed on the surface of Mn films as a  $\sim 0.02$  nm step,<sup>14</sup> where spin polarization vectors rotate  $180^\circ$  within 0.5 nm. (b) and (c) An STM image ( $V_s = -0.5$  V,  $I = 0.5$  nA,  $99 \times 99$  nm<sup>2</sup>) and an STS image (a  $dI/dV$  map at +0.1 V), respectively, which were obtained with an Fe-coated W tip positioned on the surface of the Mn films on the Fe(001) whisker. Numbers “5,” “6,” and “7” denote the local thickness in number of Mn layers at each position. Step heights are about 0.165 nm. Even and odd layers show  $dI/dV$  values of about 1.30 and 1.05 nA/V, respectively, (MR = 24%).

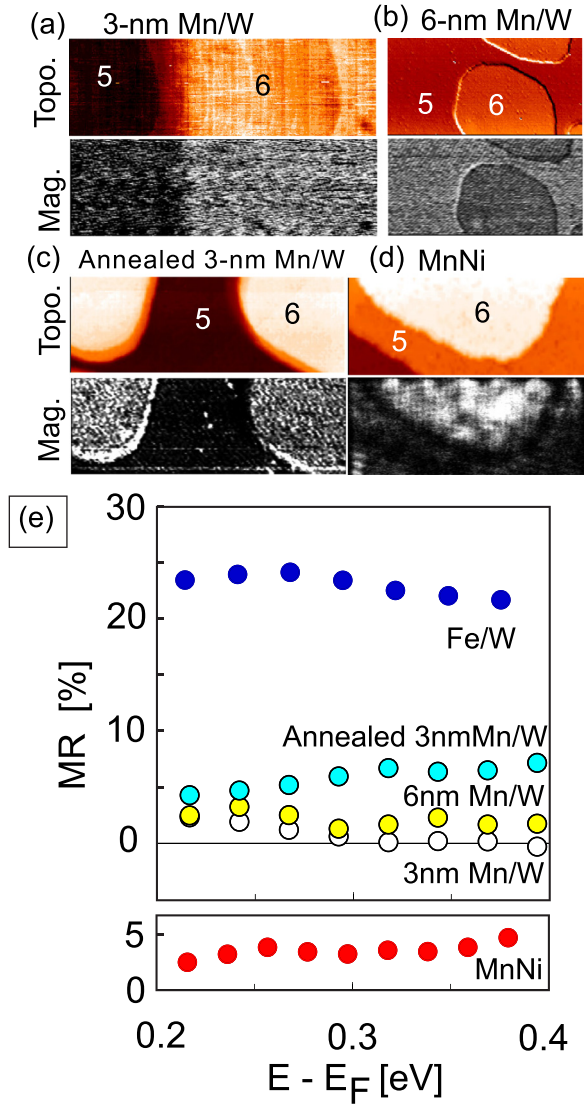


FIG. 3. (a)–(d) Spin-polarized STM images and spectroscopy maps obtained on a 5.5 ML Mn film grown on an Fe(001) with AFM Mn-coated W tips and bulk-MnNi tips, where fifth (“5”) and sixth (“6”) layers are exposed on the surface. Numbers denote the local thickness in number of Mn layers. (a) A topographic image ( $30 \times 9.5 \text{ nm}^2$ ,  $V_S = -0.5 \text{ V}$ ,  $I = 0.5 \text{ nA}$ ) and a spin-resolved  $dI/dV$  map at  $+0.2 \text{ V}$  obtained from the same area with a 3-nm Mn/W tip. At the middle, a hidden Fe step is observed (step height  $\sim 0.02 \text{ nm}$ ).  $dI/dV$  values obtained from the fifth and sixth layers are about  $0.88$  and  $0.90 \text{ nA/V}$ , respectively (MR = 2%). (b) A topographic image ( $120 \times 60 \text{ nm}^2$ ,  $V_S = -0.5 \text{ V}$ ,  $I = 0.5 \text{ nA}$ ) and a spin-resolved  $dI/dV$  map at  $+0.2 \text{ V}$  obtained from the same area with a 6-nm Mn/W tip. Fifth and sixth layers are observed as a terrace and islands, respectively.  $dI/dV$  values obtained from the fifth and sixth layers are about  $2.18$  and  $2.13 \text{ nA/V}$ , respectively (MR = 2%). (c) A topographic image ( $104 \times 36 \text{ nm}^2$ ,  $V_S = -0.5 \text{ V}$ ,  $I = 0.5 \text{ nA}$ ) and a spin-resolved  $dI/dV$  map at  $+0.2 \text{ V}$  obtained from the same area with an annealed 3-nm Mn/W tip. Fifth and sixth layers are observed as a terrace and islands, respectively.  $dI/dV$  values obtained from the fifth and sixth layers are about  $1.23$  and  $1.29 \text{ nA/V}$ , respectively (MR = 5%). (d) A topographic image ( $40 \times 16 \text{ nm}^2$ ,  $V_S = -0.5 \text{ V}$ ,  $I = 0.5 \text{ nA}$ ) and a spin-resolved  $dI/dV$  map at  $+0.2 \text{ V}$  obtained from the same area with a MnNi tip.  $dI/dV$  values obtained from the fifth and sixth layers are about  $1.74$  and  $1.79 \text{ nA/V}$ , respectively (MR = 3%). (e) Experimentally obtained MR values as a function of the sample bias. The value of  $0 \text{ eV}$  corresponds to the Fermi level. Data were obtained using 5-nm Fe- (dark blue), 3-nm Mn- (white), 6-nm Mn- (yellow), annealed 3-nm Mn-coated W tips (light blue), and the bulk-NiMn tip (red).

(a) 3-nm, (b) 6-nm, (c) annealed 3-nm Mn-coated W, and (d) bulk NiMn tips, wherein two terraces with thicknesses of five and six Mn monolayers (ML) are observed. We

performed measurements with about three to five different tips for each case. In the spin-resolved  $dI/dV$  map obtained from this area, we can clearly observe the black-white contrast between the 5- and 6-ML sections, as in the case of the Fe-coated W tip (Fig. 2). Although with all type of tips, we get magnetic contrast, the amplitude changes from tip to tip, and in Figure 3 we reproduced the maps with higher magnetic contrast for each type of tip. These spin-resolved  $dI/dV$  maps clearly show that these AFM tip electrodes are able to detect MR at 300 K.

Quantitatively, the MR value of each tip was obtained by examining the differential conductivity curves. Figure 3(e) shows the obtained MR values as a function of bias voltage, and the corresponding values are listed in Table I.<sup>31</sup> The 5-nm Fe film electrode exhibits an MR of  $23 \pm 1\%$ . The primary point of interest is that the MR is considerably smaller in the AFM tip electrodes in comparison with that in the Fe-coated tip. In particular, the Mn-coated tip with a coverage of 3 nm exhibits an extremely low MR value of  $1 \pm 1\%$ . The MR slightly increases to  $2 \pm 1\%$  when the thickness of the Mn film increases to 6 nm. These low values make these tips unsuitable for spin-resolved measurements due to the low signal-to-noise ratio.

The crystallographic ordering of Mn has the tendency of imitating the ordering of the substrate atomic structure. For example, well-ordered bcc(001) Mn films can be formed on the substrate of bcc-Fe(001) with thicknesses of more than 10 ML;<sup>24</sup> further Mn films grown uniformly on fcc-Ag(111) exhibit a hexagonal lattice symmetry.<sup>29</sup> It is well known that the apex of W tips heated at high temperature in UHV recrystallizes presenting the close-packed (110) face,<sup>25</sup> and therefore, the magnetic structures of Mn on the W tip may be examined in the light of studies of Mn on W(110). The Néel temperatures of bulk  $\alpha$ -Mn and  $\beta$ -Mn are considerably less than 300 K, while fcc  $\gamma$ -Mn and bcc  $\delta$ -Mn exhibit Néel temperatures greater than 300 K. Mn layers grow pseudomorphically on a W(110) single crystal at 300 K,<sup>30</sup> and highly strained bcc  $\delta$ -Mn layers have been observed with thicknesses of up to 3 ML, and three-dimensional islands ( $\alpha$ - or  $\delta$ -Mn) start to grow for thicker coverages, which indicates that gentle annealing assists the phase transition from  $\alpha$ -Mn or strained bcc-Mn to ordered bcc-Mn, thereby producing a higher MR. From Fig. 3(e), we note that the MR of the 3-nm Mn film increases to  $6 \pm 1\%$  after annealing.

Bulk NiMn alloy, which has a CuAu-I type face-centered tetragonal structure with lattice parameters of  $a = 3.714 \text{ \AA}$  and  $c = 3.524 \text{ \AA}$ , is an antiferromagnet. Each Mn atom has a large magnetic moment of approximately  $4 \mu_B$  and is antiferromagnetically aligned orthogonal to the  $c$ -axis

TABLE I. Magnetoresistance (MR) through the junctions and spin polarizations of the tip electrodes ( $P_{\text{tip}}$ ).

300-K MR junctions	MR (%)	$P_{\text{tip}}$ (%)
Mn(001)/vac./Fe film (5 nm)	$23 \pm 1$	$\sim 31$ (Ref. 25)
Mn(001)/vac./Mn film (3 nm)	$1 \pm 1$	$1 \pm 1$
Mn(001)/vac./Mn film (6 nm)	$2 \pm 1$	$3 \pm 2$
Mn(001)/vac./annealed Mn film	$6 \pm 1$	$9 \pm 2$
Mn(001)/vac./bulk-NiMn	$4 \pm 1$	$6 \pm 2$

(i.e., either [001] or [110]), and the Ni atoms exhibit smaller magnetic moments with values below  $0.6 \mu_B$ . These values are good for atoms in the bulk of the alloy; the size and direction of the magnetic moments as well as the spin polarization for surface atoms are unknown. For the MnNi tips, we observed MR values of  $4 \pm 1\%$ , but we were unable to control the choice of atomic species (Mn or Ni) present at the apex of the tip, which leads to a very unstable MR, i.e., the MR switches between 0% and  $4 \pm 1\%$ , with these low values these tips are not a good choice for spin-polarized measurements at RT.

The spin polarization values of these Mn-based AFM tip electrodes can be obtained by using the experimentally obtained MR values via the expression  $MR = (G_{\uparrow\downarrow}^{-1} - G_{\uparrow\uparrow}^{-1}) / G_{\uparrow\downarrow}^{-1} = 2P_{\text{sample}}P_{\text{tip}} / (1 + P_{\text{sample}}P_{\text{tip}})$ .<sup>27</sup> Since the spin polarization of the 5-nm Fe film covering the W tip ( $P_{\text{Fe-tip}}$ ) is known to be  $\sim 31\%$ ,<sup>25</sup> the spin polarization of the sample Mn(001) films can be obtained by using the expression  $P_{\text{sample}} = MR_{\text{Fe}(5\text{nm})} / (P_{\text{Fe-tip}}(2 - MR_{\text{Fe}(5\text{nm})})) = 41 \pm 2\%$ . Thus, the spin polarization of the AFM tips can be obtained via the expression  $P_{\text{AFM-tips}} = MR_{\text{AFM-tips}} / (P_{\text{sample}}(2 - MR_{\text{AFM-tips}}))$ . The obtained spin polarizations of the 3- and 6-nm Mn film tips are  $1 \pm 1\%$  and  $3 \pm 2\%$ , respectively. The annealed tip has a spin polarization of  $9 \pm 2\%$ , which is comparable to the spin polarization of Cr-coated W tips, which is  $\sim 10\%$ .<sup>22</sup> Further, we note that at 300K, AFM Cr- and Mn-coated W tips have spin polarizations that are smaller by a factor of 4 to 5 with respect to that of the FM Fe-coated W tip. The bulk-NiMn tips exhibit spin polarizations of 0% or  $5 \pm 1\%$ , and the polarizations probably depend on the chemical species (Mn or Ni) present at the apex of the tip.

In this study, quantitative 300-K spin polarization values of Mn-based AFM tip electrodes were obtained by measuring MR with a spin-polarized STM setup in ultrahigh vacuum (UHV). Mn-coated W and bulk-NiMn tips were used in the experiments. All the tips exhibit MR at 300 K, and the MR values of the W tips covered by Mn films with thicknesses of 3 and 6 nm exhibit MR values of only  $1 \pm 1\%$  and  $2 \pm 1\%$ ; however, increasing the crystalline quality of the Mn film by annealing increases the MR to  $6 \pm 1\%$ . We obtained spin polarizations of  $1 \pm 1\%$ ,  $3 \pm 2\%$ , and  $9 \pm 2\%$  for 3-nm, 6-nm, and annealed 3-nm Mn-coated W tips, respectively. The results demonstrate that the crystallographic quality of the films is crucial to obtain stable MR as well as spin polarization at 300 K. The annealed tip has a spin polarization comparable to that the Cr-coated W tips, which value is  $\sim 10\%$ .<sup>22</sup> It is observed that at 300 K, AFM Cr- and Mn-coated W tips exhibit spin polarizations that are smaller by a factor of 4 to 5 with respect to that for the FM Fe-coated W tip. Bulk-NiMn tips exhibit an MR of  $4 \pm 1\%$  and spin polarization of  $6 \pm 2\%$ , but it can switch to 0%, which is probably because the choice of chemical species at the apex of the tip cannot be controlled.

Kind guidance for chemical vapor deposition for Fe whiskers by Dr. D. T. Pierce is acknowledged. We thank Professor Dr. I. V. Shvets and Dr. S. F. Ceballos for helpful discussions for assistance in the preparations of MnNi tips. Careful measurements were realized with the support of Professor Dr. H. van Kempen. We thank Dr. L. Gerhard and

Mr. N. K. M. Nazriq for carefully reading our manuscript. This work was supported by JSPS KAKENHI Grant Nos. 23681018 and 25110011, Japan Science and Technology Agency (JST)-Improvement of Research Environment for Young Researchers: Chiba University Young Research-Oriented Faculty Member Development Program in Bioscience Areas, Chiba Univ. Global COE Program: Advanced School for Organic Electronics, Casio Science Promotion Foundation, Asahi Glass Foundation, Hatakeyama Culture Foundation, The Association for the Progress of New Chemistry, Iketani Science and Technology Foundation, The Noguchi Institute, Ozawa Yoshikawa Memorial Electronics Foundation, Research Foundation for the Electrotechnology of Chubu, The Nakajima Foundation, The Futaba Electronics Memorial Foundation, and the Shimadzu Foundation. Spanish government through the MICINN Project FIS2012-18847 and the Comunidad the Madrid through Project NANOBIOMAGNET S2009/MAT1726.

<sup>1</sup>T. Maruyama, Y. Shiota, T. Nozaki, K. Ohta, N. Toda, M. Mizuguchi, A. A. Tulapurkar, T. Shinjo, M. Shiraishi, S. Mizukami, Y. Ando, and Y. Suzuki, *Nat. Nanotechnol.* **4**, 158 (2009).

<sup>2</sup>W.-G. Wang, M. Li, S. Hageman, and C. L. Chien, *Nat. Mater.* **11**, 64 (2012).

<sup>3</sup>L. Gerhard, T. K. Yamada, T. Balashov, A. F. Takacs, R. J. H. Wesselink, M. Däne, M. Fechner, S. Ostanin, A. Ernst, I. Mertig, and W. Wulfhchel, *Nat. Nanotechnol.* **5**, 792 (2010).

<sup>4</sup>S. Schmaus, A. Bagrets, Y. Nahas, T. K. Yamada, A. Bork, M. Bowen, E. Beaurepaire, F. Evers, and W. Wulfhchel, *Nat. Nanotechnol.* **6**, 185 (2011).

<sup>5</sup>A. Bagrets, S. Schmaus, A. Jaafar, D. Kramczynski, T. K. Yamada, M. Alouani, W. Wulfhchel, and F. Evers, *Nano Lett.* **12**, 5131 (2012).

<sup>6</sup>S. L. Kawahara, J. Lagoute, V. Repain, C. Chacon, Y. Girard, S. Rousset, A. Smogunov, and C. Barreteau, *Nano Lett.* **12**, 4558 (2012).

<sup>7</sup>V. M. Karpan, G. Giovannetti, P. A. Khomyakov, M. Talanana, A. A. Starikov, M. Zwierzycki, J. van den Brink, G. Brocks, and P. J. Kelly, *Phys. Rev. Lett.* **99**, 176602 (2007).

<sup>8</sup>R. Wiesendanger, M. Bode, and M. Getzlaff, *Appl. Phys. Lett.* **75**, 124 (1999).

<sup>9</sup>M. Bode, O. Pietzsch, A. Kubetzka, S. Heinze, and R. Wiesendanger, *Phys. Rev. Lett.* **86**, 2142 (2001).

<sup>10</sup>O. Pietzsch, A. Kubetzka, M. Bode, and R. Wiesendanger, *Phys. Rev. Lett.* **84**, 5212 (2000).

<sup>11</sup>T. K. Yamada, M. M. J. Bischoff, G. M. M. Heijnen, T. Mizoguchi, and H. van Kempen, *Phys. Rev. Lett.* **90**, 056803 (2003).

<sup>12</sup>T. K. Yamada, M. M. J. Bischoff, G. M. M. Heijnen, T. Mizoguchi, and H. van Kempen, *Jpn. J. Appl. Phys., Part 1* **42**, 4688 (2003).

<sup>13</sup>U. Schlickum, N. Janke-Gilman, W. Wulfhchel, and J. Kirschner, *Phys. Rev. Lett.* **92**, 107203 (2004).

<sup>14</sup>T. K. Yamada, E. Martinez, A. Vega, R. Robles, D. Stoeffler, A. L. Vazquez de Parga, T. Mizoguchi, and H. van Kempen, *Nanotechnology* **18**, 235702 (2007).

<sup>15</sup>M. Kleiber, M. Bode, R. Ravlic, and R. Wiesendanger, *Phys. Rev. Lett.* **85**, 4606 (2000).

<sup>16</sup>A. Kubetzka, M. Bode, O. Pietzsch, and R. Wiesendanger, *Phys. Rev. Lett.* **88**, 057201 (2002).

<sup>17</sup>T. Matsuda, A. Tonomura, T. K. Yamada, D. Okuyama, N. Mizuno, A. L. Vazquez, V. de Parga, H. van Kempen, and T. Mizoguchi, *IEEE Trans. Magn.* **41**, 3727 (2005).

<sup>18</sup>H. F. Ding, W. Wulfhchel, U. Schlickum, and J. Kirschner, *Europhys. Lett.* **63**, 419 (2003).

<sup>19</sup>A. Li Bassi, C. S. Casari, D. Cattaneo, F. Donati, S. Foglio, M. Passoni, C. E. Bottani, P. Biagioni, A. Brambilla, M. Finazzi, F. Ciccacci, and L. Duo, *Appl. Phys. Lett.* **91**, 173120 (2007).

<sup>20</sup>M. Corbetta, S. Ouazi, J. Borne, Y. Nahas, F. Donati, H. Oka, S. Wedekind, D. Sander, and J. Kirschner, *Jpn. J. Appl. Phys., Part 1* **51**, 030208 (2012).

<sup>21</sup>G. Rodary, J.-C. Girard, L. Largeau, C. David, O. Manguin, and Z.-Z. Wang, *Appl. Phys. Lett.* **98**, 082505 (2011).

<sup>22</sup>S. Nagai, K. Hata, H. Oka, D. Sander, and J. Kirschner, *Appl. Phys. Express* **7**, 025204 (2014).

- <sup>23</sup>H. Yang, A. R. Smith, M. Prikhodko, and W. R. L. Lambrecht, *Phys. Rev. Lett.* **89**, 226101 (2002).
- <sup>24</sup>T. K. Yamada, M. M. J. Bischoff, T. Mizoguchi, and H. van Kempen, *Surf. Sci.* **516**, 179 (2002).
- <sup>25</sup>T. Irisawa, T. K. Yamada, and T. Mizoguchi, *New J. Phys.* **11**, 113031 (2009).
- <sup>26</sup>Y. Yamagishi, S. Nakashima, K. Oiso, and T. K. Yamada, *Nanotechnology* **24**, 395704 (2013).
- <sup>27</sup>Y. Qi, D. Y. Xing, and J. Dong, *Phys. Rev. B* **58**, 2783 (1998).
- <sup>28</sup>T. K. Yamada, M. M. J. Bischoff, T. Mizoguchi, and H. van Kempen, *Appl. Phys. Lett.* **82**, 1437 (2003).
- <sup>29</sup>C. L. Gao, W. Wulfhekel, and J. Kirschner, *Phys. Rev. Lett.* **101**, 267205 (2008).
- <sup>30</sup>M. Bode, M. Hennefarth, D. Haude, M. Getzlaff, and R. Wiesendanger, *Surf. Sci.* **432**, 8 (1999).
- <sup>31</sup>All data were obtained using the same bias voltage ( $V_s = -0.5$  V) and tunneling current ( $I = 0.5$  nA) to stabilize the distance between the tip and sample before disconnecting the feedback loop to acquire the  $dI/dV$  curves in order to avoid the dependence of the magnetic contrast on the tip-sample separation.<sup>11</sup> Since the spin polarization values for Mn(001) are well characterized and almost constant above the Fermi level,<sup>11</sup> we measured magnetoresistance values between +0.2 to +0.4 eV.